Journal of CO2 Utilization 83 (2024) 102820

Contents lists available at ScienceDirect

Journal of CO2 Utilization

journal homepage: www.elsevier.com/locate/jcou

Improving the performance of gliding arc plasma-catalytic dry reforming via a new post-plasma tubular catalyst bed

Wencong Xu [a,b,c,*], Lukas C. Buelens [c], Vladimir V. Galvita [c], Annemie Bogaerts [b], Vera Meynen [a]

[a] Laboratory of Adsorption and Catalysis, Department of Chemistry, University of Antwerp (CDE), Universiteitsplein 1, Wilrijk, Antwerp B-2610, Belgium
[b] Plasma Lab for Applications in Sustainability and Medicine-Antwerp, Department of Chemistry, University of Antwerp (CDE), Universiteitsplein 1, Wilrijk B-2610, Belgium
[c] Laboratory for Chemical Technology, Department of Materials, Textiles and Chemical Engineering, Ghent University, Technologiepark 125, Ghent B-9052, Belgium

ARTICLE INFO

Keywords:
Dry reforming
Gliding arc plasma
Plasma catalytic DRM
Ni-based mixed oxide
Post-plasma catalysis

ABSTRACT

A combination of a gliding arc plasmatron (GAP) reactor and a newly designed tubular catalyst bed (N-bed) was applied to investigate the post-plasma catalytic (PPC) effect for dry reforming of methane (DRM). As comparison, a traditional plasma catalyst bed (T-bed) was also utilized. The post-plasma catalytic effect of a Ni-based mixed oxide (Ni/MO) catalyst with a thermal catalytic performance of 77% CO_2 and 86% CH_4 conversion at 700 ℃ was studied. Although applying the T-bed had little effect on plasma based CO_2 and CH_4 conversion, an increase in selectivity to H_2 was obtained with a maximum value of 89% at a distance of 2 cm. However, even when only α-Al_2O_3 packing material was used in the N-bed configuration, compared to the plasma alone and the T-bed, an increase of the CO_2 and CH_4 conversion from 53% and 53% to 69% and 69% to 83% was achieved. Addition of the Ni/MO catalyst further enhanced the DRM reaction, resulting in conversions of 79% for CO_2 and 91% for CH_4. Hence, although no insulation nor external heating was applied to the N-bed post plasma, it provides a slightly better conversion than the thermal catalytic performance with the same catalyst, while being fully electrically driven. In addition, an enhanced CO selectivity to 96% was obtained and the energy cost was reduced from ~ 6 kJ/L (plasma alone) to 4.3 kJ/L. To our knowledge, it is the first time that a post-plasma catalytic system achieves this excellent catalytic performance for DRM without extra external heating or insulation.

1. Introduction

Simultaneously converting CH_4 and CO_2 through dry reforming of methane (DRM) has been a topic of significant interest for researchers worldwide for decades [1–3]. Due to the high stability of CO_2 molecules, the reaction is endothermic ($CO_2 + CH_4 \rightarrow 2CO + 2H_2$, $\Delta H^0 = 247 kJ/mol$) which requires the reaction to usually happen at high temperatures over 700 °C. Furthermore, during the reaction, carbon deposition on the catalyst and catalyst sintering will cause deactivation of the catalyst, limiting its further industrial application [1].

Among the various types of technologies to improve the state of the art, plasma, the fourth state of matter containing reactive species (electrons, ions, radicals, and excited molecules), provides a particularly unique pathway as it can use flexible and renewable electrical energy sources, and can relatively easily be scaled up [4–7]. In its simplest case, plasma is a (partially) ionized gas, which is produced by gas flowing between two electrodes between which there is an electric potential difference. This causes gas breakdown, and the creation of free electrons and ions. The electrons collide with the gas molecules, producing also other reactive species, such as radicals and excited molecules. This chemical species cocktail creates a reactive environment that facilitates the dissociation of stable molecules, such as CO_2 and CH_4 under DRM conditions [8]. The product obtained from the plasma DRM reaction mainly contains syngas (H_2/CO), as well as hydrocarbons and oxygenates [8–13]. Extensive investigation for plasma-based DRM has been done with various types of plasma technologies, such as dielectric barrier discharge (DBD) [10,14–19], radio-frequency (RF) discharges [20–22], glow discharges [13,23], microwave (MW) discharges [24–27], corona discharges [28,29], and gliding arc (GA) discharges [8,30–35]. It is worth to note that the GA plasma is a promising plasma type for DRM, as it can generate electrons with an energy of around 1 eV, which is ideal for the CO_2 vibrational excitation during the dissociation

* Corresponding author at: Laboratory of Adsorption and Catalysis, Department of Chemistry, University of Antwerp (CDE), Universiteitsplein 1, Wilrijk, Antwerp B-2610, Belgium.
E-mail address: wencong.xu@uantwerpen.be (W. Xu).

https://doi.org/10.1016/j.jcou.2024.102820
Received 12 February 2024; Received in revised form 21 May 2024; Accepted 21 May 2024
Available online 25 May 2024

process [31,36,37].

However, the classical two-dimensional (2D) GA plasma is still facing limitations, such as limited conversion of 10–40%, because a considerable fraction of feed gas does not pass through the plasma region [37–41]. Therefore, new designs were developed with improvements of cylindrical electrodes and tangential gas entrances, which allow the formation of a vortex flow, resulting in longer residence times and eventually higher conversions of 14–65% [8,30–32,42,43]. Among them, a gliding arc plasmatron (GAP), developed by Nunnally et al. [44], showed high potential for DRM [8,30,31]. Nevertheless, the highest conversion is still in the range of 40–60% in the plasma alone case [30], which is lower than the typical value of around 90% achieved in thermal catalytic DRM at high temperatures above 750 °C [45–47]. Therefore, a method to improve its plasma performance is needed. Implementing a catalyst bed after the plasma, forming a post-plasma catalytic (PPC) system, can possibly further improve the gas conversion.

Currently, for this type of GAP setup, no systematic study on PPC DRM was performed. But lessons can be learnt from other types of GA PPC DRM systems. Zhang et al. [48] showed by means of simulation that after adding the catalyst bed, a strong backflow of gas above the catalyst bed occurred, which partly flowed back to the plasma area, where it was further treated by the plasma. Li et al. [49] investigated the relation between distance and temperature in a GA plasma system and summarized how the distance between a catalyst bed and plasma affected the results of reforming of biogas with feed gas molar ratio of CH_4:CO_2:O_2 = 3:2:1.8. They found that the catalyst mid-bed temperature elevated from 647 °C to 779 °C as the distance between the catalyst bed and the top of the plasma reactor cylinder decreased from 11 to 4 cm, which was attributed to the decrease of heat loss from the GA plasma when approaching the plasma area. Consequently, the conversions of CH_4 and CO_2 increased from 82% and 82% to 92% and 2% to 20%, respectively [49].

Martin-Del-Campo et al. [42] recently investigated the performance of DRM in a rotating gliding arc (RGA) plasma coupled with a spouted bed reactor system with and without catalyst. The authors found that the conversions of CO_2 and CH_4 for plasma alone were higher than those with catalyst. A possible reason was that the presence of a catalyst bed filled with materials interfered with the arc formation, which limited the formation of active species produced by the plasma [42]. On the contrary, in another study reported by Zhu et al. [34], an enhancement in the conversion of CH_4 from 52.6% to 58.5% was observed when the RGA plasma was combined with a Ni/γ-Al_2O_3 catalyst loaded with 10 wt% Ni, compared with plasma alone for DRM. However, the presence of the catalyst had almost no effect on the CO_2 conversion. Moreover, Liu and co-workers [50] reported that supplying extra heat to the catalyst reactor after plasma could be a possible way to improve the GA plasma-catalytic system. Compared to warm plasma alone (WP) (no catalyst), warm plasma catalysis without heating (WPC-NH) resulted in almost the same conversions of CO_2 and CH_4, suggesting that the Ni-based catalyst did not contribute to the DRM reaction, although it had good performance in the conventional thermal catalytic (CC) case. This was due to the low temperature of the after-plasma gas flow, which was only in the range of 350 °C to 500 °C, at which the Ni-based catalyst is inactive for DRM. Once extra heating was added at a temperature of 850 °C, the warm plasma catalysis with heating (WPC) case exhibited the highest conversions for both CO_2 and CH_4. Moreover, these values increased as the feed gas flow rate decreased, resulting in 94% CH_4 conversion and 91% CO_2 conversion at a gas hourly space velocity (GHSV) of 3200 h^{-1}. In another newly reported paper, Lian et al. [51] compared warm plasma coreforming of dilute bioethanol and methane to produce hydrogen, with the warm plasma-catalysis case, in which extra heating at 800 °C improved the carbon conversion from 66% to 97%, the hydrogen yield from 55% to 78% and the energy efficiency from 80% to 85%. Their research suggested the importance of extra heating in the warm plasma catalytic system, which also proves that temperature is an importance issue for post-plasma catalysis. Thus, the question comes up whether there is a solution able to transfer more heat from the plasma to the catalyst and improve the catalytic conversion, without any extra heating? This would indeed be the ultimate goal to obtain a fully electrically driven processes including heat (energy) integration of the plasma to the post-plasma catalyst [52].

In the present study, a Ni-based mixed oxide (Ni/MO) catalyst derived from LDH (layered double hydroxide), which was reported to have a good performance in thermal catalytic DRM [53], was coupled with a GAP reactor for DRM. Different from the traditional tray type catalyst bed (T-bed) used behind the GAP reactor, we propose a newly designed tubular catalyst bed (N-bed) with the purpose to enhance heat and mass transfer of the plasma exhaust to the post-plasma catalyst bed, as this was hypothesized as the key reason for the absence of catalytic performance as introduced in the introduction part. Therefore, the N-bed was directly connected to the plasma chamber and positioned inside the post-plasma quartz tube, forming a double wall effect, which was hypothesized to avoid the need for insulation or external heating. Finally, we compared our experimental results with the thermal catalysis using the same catalyst and the state-of-the art, illustrating the potential for further improvement in the post-plasma catalysis system.

2. Experimental

2.1. Catalyst preparation and characterization

The support of MgAl-LDH was synthesized via the co-precipitation method as reported [54]. Then, 10 wt% Ni was loaded on the MgAl-LDH via the wet impregnation method, by contacting, the MgAl-LDH with $Ni(NO_3)_2.6\ H_2O$ solution for 12 h while stirring, after which the Ni/MgAl-LDH was dried at 80 ℃ overnight and calcined at 800 °C for 6 h. The obtained Ni/MgAl mixed metal oxide (denoted as NiO/MO) powder was pressed into tablets at 5 MPa. Then, the tablets were crushed and sieved into a size of 0.4–0.6 mm.

Based on the H_2-TPR profile (Fig. 2B), the sample already started to be reduced at 700 °C. Moreover, calcination was done at 800 °C with the aim to prevent increased aggregation. Therefore, we decided to reduce the sample at the same temperature as for calcination, being 800 °C for a duration of 6 h with a 2% H_2/Ar gas at a flow rate of around 100 mL/min, a heating rate of 10 °C/min, before they were applied for reaction. α-Al_2O_3 spheres (Alfa Aesar, 3/16 in.) were crushed and sieved into the same size fraction to be utilized as filling material. Before being used for reaction, the reduced catalyst Ni/MO and α-Al_2O_3 were uniformly mixed in a bottle. For a fair comparison, both thermal and GAP catalytic DRM were performed at the same GHSV of 480 $L{\cdot}g_{cat}^{-1}{\cdot}h^{-1}$.

XRD, and H_2-TPD were done for the catalyst before being used for the reaction. TG-MS was conducted for the catalyst after the DRM reaction to analyze the weight loss and carbon deposition of the used-catalyst. The details for these characterizations are given in the supporting information.

2.2. Thermal catalytic DRM

To compare with the plasma-catalytic DRM, the Ni/MO catalyst was also used in thermal catalytic DRM tests. For these experiments, the catalyst size fraction was 0.25–0.4 mm, considering the size of the quartz tube reactor used. 10 mg unreduced NiO/MO material and 100 mg α-Al_2O_3 with the same size fraction were mixed uniformly before they were filled into a quartz tube fixed bed reactor supported on quartz wool. Before starting the DRM reaction, the uniform mixture was reduced by 20% H_2/Ar with a flow rate of 80 mL/min at 800 °C for 0.5 h. Then, the gas was changed to pure Ar with the same gas flow rate for another 0.5 h. To start the reaction, the gas was changed to a ratio of Ar:CO_2:CH_4 = 8:1:1 with total gas flow rate of 80 mL/min to keep the same GHSV as in the plasma catalysis condition. After reduction of the catalyst and flushing by Ar, the catalytic activity was measured at discrete temperature steps. Usually, for fixed bed thermal catalytic DRM,

the experiments are performed by increasing temperature which takes less time. However, potential carbon deposition and accumulation at low temperature could significantly affect the catalytic activity. In our study, the high temperature catalytic performance is the most important data, which we need for comparison with the results under post-plasma catalysis conditions. Therefore, to avoid any loss of catalytic activity during DRM from low temperature tests, we have chosen to start with the reaction at high temperature. The temperature was decreased point by point from 800 to 400 °C and pure Ar was utilized during the temperature decreasing process. At each temperature point, the reaction was maintained for more than one hour and during this period the outlet gas was collected and analyzed by a Thermo Scientific Trace 1300 GC.

2.3. Plasma-catalytic DRM

Schematic diagram of the GAP DRM experimental setup is given in Fig. S1. The GAP device was described in detail before [36,55,56]. Mixed gas was supplied to the plasma with a composition of N_2:CH_4:CO_2 = 8:1:1 (or 8:0.6:1) at a total gas flow rate of 8 L/min (Air Liquide, N_2 purity 99.999%, CO_2 purity 99.998%, and CH_4 purity 99.995%). The flow rate of each gas was controlled by Bronkhorst mass flow controllers. The plasma in the GAP was generated by applying a high voltage to the cathode with a DC power supply (APS – Advanced Plasma Solutions). The voltage and current of the plasma were measured by a high-voltage probe (Pintek HVP-15HF) and a current sense resistor of 3 Ω. The data of voltage and current were collected by a two channels digital storage oscilloscope (Tektronix TDS 2012C). The current used for the plasma was 0.25 A and a voltage around 0.6–0.8 kV was obtained. The plasma power was calculated based on the measured voltage and current.

The post-plasma reactor tube was made of quartz with an inside diameter of 6.4 cm. There are six outlets at different positions on the reactor with a diameter of 1 cm to allow extra gas to be added through them or implement thermocouples. Herein, they were all sealed by valves during the reaction process. A thermocouple is placed after the catalyst bed through the first outlet to record the temperature of the gas that passes through the catalyst bed. The distance from the thermocouple to the top of the quartz reactor is 4.9 cm (Fig. 1 C). To add the catalyst just after the post-plasma exhaust, we developed a newly designed tubular catalyst bed (N-bed), as shown in Fig. 1A-B. Detailed pictures are shown in Fig S2. The N-bed is directly connected to the anode of the plasma reactor by a stainless steel connector (detailed photographs, see Fig. S2A-B). A tubular body with a diameter of 3.5 cm and height of 4.5 cm was utilized and at the bottom a mesh was stacked inside where the catalyst can be placed on. As comparison, the traditional catalyst bed (T-bed) was also utilized (Fig. 1 C), which was made of a metal ring combined with a mesh tray and which can be adjusted in height closer or further from the plasma exhaust. The distance between the T-bed and the plasma varied from 2 cm to 4 cm and the reaction conditions were denoted as T-bed-l, where l is the distance in centimeter.

For the plasma-catalytic DRM reaction, 1 g reduced catalyst with 4 g α-Al_2O_3 filling material was mixed uniformly and placed in/on the catalyst bed for both configurations. In comparison, plasma alone or with 5 g α-Al_2O_3 filling material only was also tested at the same reaction conditions. A total gas flow rate of 8 L/min with composition of N_2:CO_2:CH_4 = 8:1:1 was applied to generate the plasma. A gas hourly space velocity (WHSV) of 480 $L{\cdot}g_{cat}^{-1}{\cdot}h^{-1}$ was obtained. Besides this, with the same gas flow rate, a lower CH_4/CO_2 ratio of 0.6 was also tested. Furthermore, a blank experiment with only the N-bed was performed in this ratio. After starting the plasma, gas data was collected by a Thermo Scientific/Interscience Trace 1300 Gas Chromatograph (GC).

2.4. Gas analysis

For the plasma-catalytic DRM system, the products were analyzed by the trace GC. Nitrogen was used as internal standard gas. The definitions and formulas to calculate the conversions, carbon-based selectivity (for CO, C_2H_2, and C_2H_4) and carbon balance, hydrogen-based selectivity (for H_2), yield, specific energy input (SEI), and energy cost (EC) are shown in supplementary information.

3. Results and discussion

3.1. Catalyst characterization

The XRD patterns of as-prepared Ni-LDH and the Ni/MO catalyst (after calcination and reduction) are shown in Fig. 2 A. For the Ni-LDH, peaks at 11.3°, 22.9°, 34.8°, 39.3°, 46.6°, 61.8° and 63.1° were noted, confirming the successful synthesis of the Ni-LDH phase. The introduction of Ni did not alter the LDH structure. The Ni/MO catalyst, produced after calcination and reduction, exhibited XRD patterns with peaks of Ni^0 at 2θ values of 44.3°, 51.7° and 76.3°. Additionally, phases of MgO and NiO were detected in the Ni/MO catalyst. The appearance of NiO in the reduced Ni/MO can be either due to a partial reoxidation of the Ni during the measurement or/and incomplete reduction of the NiO/MO sample as the sample was reduced at 800 °C, similar to the calcination temperature.

The H_2-TPR was conducted to examine the reduction behaviour and

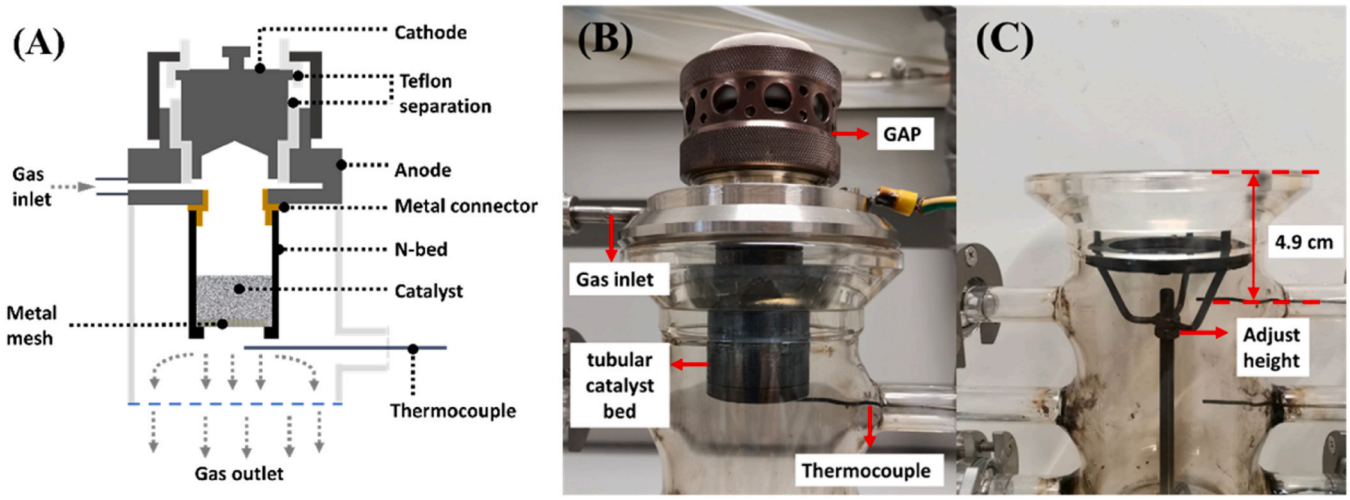

Fig. 1. (A) Schematic description of the newly designed tubular catalyst bed (N-bed), (B) photograph of the N-bed connected to the plasma-catalytic system, and (C) photograph of the traditional catalyst bed (T-bed) used in the plasma-catalytic system.

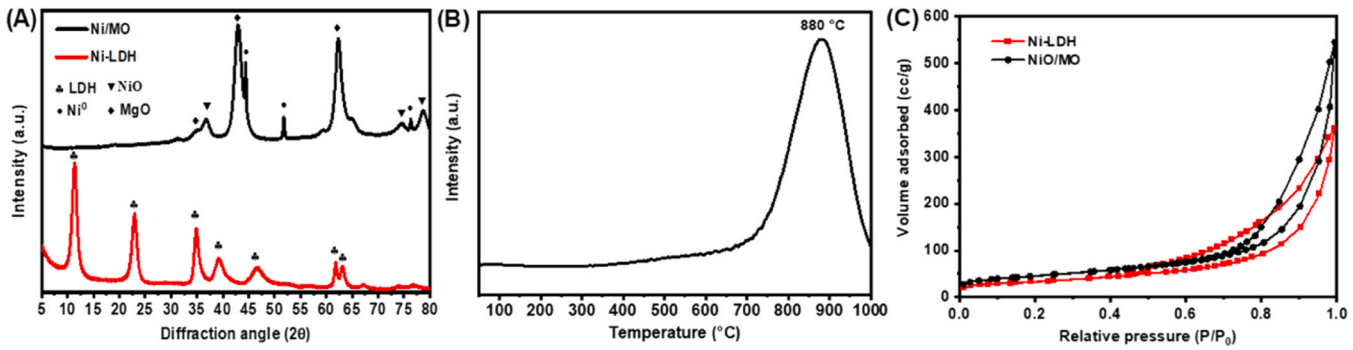

Fig. 2. (A) XRD patterns of the Ni-LDH and reduced Ni/MO; (B) H_2-TPR of the calcined NiO/MO, and (C) nitrogen adsorption-desorption isotherms at -196 °C of the as-prepared Ni-LDH and the obtained NiO/MO after calcination.

the interaction between Ni and the support, as shown in Fig. 2B. The TPR results revealed a single wide peak centered at approximately 880 °C, attributed to the reduction of Ni^{2+} species in the metal oxide to Ni^0 [57]. The absence of other peaks indicates a uniform distribution of Ni and the lack of bulk crystallite NiO species formation.

After calcination, a nickel-based mixed oxide (NiO/MO) was obtained. The surface area, porous and textural properties of the Ni-LDH and NiO/MO were measured by N_2 sorption. Fig. 2 C shows the N_2 sorption isotherm of the Ni-LDH and NiO/MO samples. The change in hysteresis at relative pressures > P/P_0 0.45 suggests the change in morphology of the particles after calcination from a plate-like morphology to small particles with interstitial porosity. The apparent BET specific surface area of Ni-LDH was 117 m^2/g. After calcination the resulting NiO/MO exhibited a larger specific surface area of 178 m^2/g. This increase is attributed to the collapse of the layered structure and the loss of interlayer molecules or anions.

3.2. Thermal catalytic activity

To provide a benchmark for the post-plasma catalysis, the catalyst was evaluated towards its thermal catalytic DRM performance. The thermal catalytic performance of the Ni/MO catalyst at various temperatures is shown in Fig. 3. To isolate the impact of the α-Al_2O_3 filling material from the catalytic effect, an experiment was conducted using 110 mg of α-Al_2O_3 following the same procedure. As shown in Fig. 3, both CO_2 and CH_4 showed 0% conversion in the temperature range of 400–800 °C. This confirms that α-Al_2O_3 has no catalytic effect on DRM within this temperature range. For the catalyst, its catalytic activity of

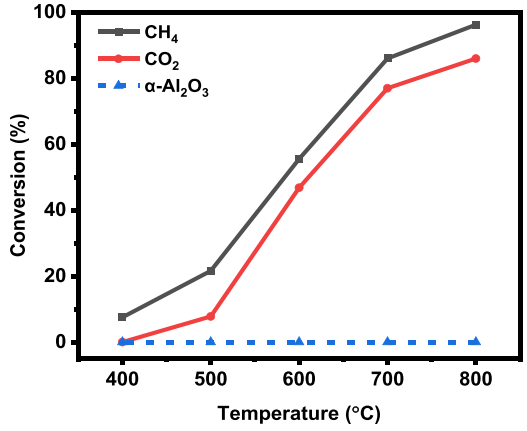

Fig. 3. CH_4 and CO_2 conversions by the Ni/MO catalyst and α -Al_2O_3 during the thermal catalytic DRM reaction at different temperatures. In the α-Al_2O_3 case, the 10 mg catalyst was replaced by 10 mg α-Al_2O_3. Experimental conditions: catalyst: 10 mg, gas flow rate: 80 mL/min (GHSV = 480 $L{\cdot}g_{cat}^{-1}{\cdot}h^{-1}$), gas composition: $Ar:CO_2:CH_4$ = 8:1:1.

the catalyst enhanced as the temperature increased. Maximum conversions of CO_2 and CH_4 of 86% and 96% were obtained at 800 ℃, which decreased to 77% and 86% for CO_2 and CH_4 as the temperature decreased to 700 ℃. The selectivity of CO and H_2 (see Table S1), however, did not change and remained around 88% for CO and 100% for H_2. Moreover, the H_2/CO ratio was 0.9 in both conditions. Usually, if a side reaction due to the reverse water gas shift reaction (RWGS, $CO_2 + H_2 \rightarrow CO + H_2O$, $\Delta H^0 = 41 kJ/mol$) would happen in the DRM process, the conversion of CO_2 would be expected to be higher than that of CH_4. However, the conversion of CH_4 consistently exceeded that of CO_2 at all temperature points measured. This higher CH_4 conversion can be attributed to the direct CH_4 decomposition, forming coke, which blocks the active sites needed for CO_2 activation [58]. Although methane decomposition occurs at temperatures from 600 °C to over 1000 °C, depending on the method and catalyst presence. The Boudouard reaction ($2CO \rightarrow C + CO_2$, $\Delta H^0 = -172 kJ/mol$) is another key side reaction. This reaction is expected to be less favored above 700 °C due to the positive Gibbs free energy change, which indicates a shift in favorability towards methane decomposition at higher temperatures [59–61]. The high CO selectivity (100%) observed below 600 °C suggests limited occurrence of the Boudouard reaction, likely due to high CO_2/CO ratios at low CO_2 conversions and/or kinetic limitations, as shown in Table S1. The decrease in CO selectivity to 92% at 600 °C and 89% at 700 °C can be linked to increased carbon formation via the Boudouard reaction and the commencement of thermal methane decomposition around 600 °C. At 800 °C, the methane decomposition likely becomes the predominant factor in reducing CO selectivity to 88%.

3.3. GAP plasma-catalytic activity

The T-bed with adjustable distance between the plasma and catalyst was applied, in addition to the N-bed configuration. To study the potential catalytic performance of the catalyst, excluding the filling effect of the post-plasma bed itself, experiments were compared with tests using only α-Al_2O_3 at the same total amount. Besides this, in the T-bed configurations, to keep the heat produced by plasma in the reactor, aluminum silicate insulation cotton was wrapped around the T-bed reactor as shown in Fig. S3 (for the N-bed configurations, no insultation or external heating was added). The performance of plasma-catalytic DRM in the T-bed configuration is shown in Fig. S4, which suggested no obvious improvement with the addition of insulation. Moreover, considering carbon deposition on the catalyst in the early plasma stage, which may lead to the deactivation of the catalyst and a decrease in the plasma-catalytic performance, a lower CH_4/CO_2 ratio of 0.6 was also tested in both T-bed and N-bed cases and compared to a ratio of 1, to study how it affected the results. These results are shown in the Fig. S5-S6 and discussed at the end of Section 3.3.1 in comparison with the results with a ratio of 1:1.

3.3.1. Plasma-catalytic DRM with CH_4/CO_2 ratio of 1

The conversions (left y-axis) of CO_2 and CH_4 for DRM in the GAP plasma-catalytic system and the at CH_4/CO_2 ratio of 1 are shown in Fig. 4. These results illustrate that by adding the catalyst at a distance of 2 cm (T-bed-2 Ni/MO), the conversion of CO_2 kept almost unchanged around 53–54%, while the CH_4 conversion decreased from 66% to 63%. Increasing the distance between the catalyst bed and the plasma from 2 cm to 3 cm, both the conversion of CO_2 and CH_4 increased a bit to 55% for CO_2 and 65% for CH_4, while the increase of CO_2 was within the error range. Although the increase of the CH_4 conversion was higher than the error (from 63% to 65%), it was still slightly lower (65% vs 66%) compared to the plasma alone configuration. When moving the distance further away from the plasma exhaust to 4 cm, however, the CO_2 and CH_4 conversion became similar to the pure plasma case. The different tendency changes for CO_2 and CH_4 in the T-bed cases could imply that a possible backflow to some degree was beneficial for CO_2 but inhibited to some extent the CH_4 dissociation, but further research is needed to confirm this. The decreasing effect of Ni-based catalysts (loaded on Al_2O_3 and SiO_2) on the conversions in plasma-catalytic DRM in a GA plasma system was also reported in literature [43]. The influence disappeared when the distance of the T-bed to the plasma exhaust was increased to 4 cm, which could be due to a weakened effect of the backflow. Changing the catalyst to filling material of α-Al_2O_3 and comparing it with Ni/MO at 4 cm distance showed no obviously changes in conversion, which implies that the catalyst had no catalytic activity at this distance.

As suggested by the thermal catalytic DRM results shown in Fig. 3 and the literature [62], higher temperatures benefit the catalyst to improve the DRM results. Therefore, a comparison experiment with insulation material wrapping around the reactor to avoid heat losses was conducted in the T-bed configuration (see photographs of the reactor in Fig. S3B). After being wrapped with insulation material, the temperature after the catalyst bed increased (Fig. S3C), although it remained limited to about 450 °C. However, when looking at the conversion and selectivity, no improvement was achieved (Fig. S4), as the temperature still remains too low compared to what is needed to thermally activate the catalyst (Fig. 3).

Therefore, a new catalyst bed (N-bed) was designed to collect more heat from the GAP device, by directly connecting it with a metal connector to the plasma reactor segment and forming a double-walled configuration with the quartz tube around the smaller N-bed connected to the plasma, hypothesized as a means to prevent the need for external heating and insulation material to be added. As shown in the Fig. 4, once the N-bed configuration was applied, even when only α-Al_2O_3 was used, the conversion of both CO_2 and CH_4 increased to 69% for CO_2 and 83% for CH_4. This cannot be due to catalytic activity, as it was proven that α-Al_2O_3 did not exhibit catalytic effects in previous studies. Therefore, we believe this is attributed to differences in the flow behaviour such as strong backflow, caused by the special design of the N-bed. Due to the sealed tubular body, all the gas is forced to go through the filling material before expanding in the wider quartz tube, and due to blocking effects (i.e., a slight increase in the feed gas pressure from about 0.25 bar to 0.3 bar, which was measured by a pressure gauge, shown in experimental setup in Fig. S1) by the catalyst bed, more gas is expected to form a stronger backflow, possibly resulting in a longer residence time for the reactants as well as radicals formed in the plasma region, which could explain the higher conversions. Although, as reported by Zhang et al. [48], the addition of a T-bed can cause backflow as well, the unsealed side part of the T-bed can give a pathway for the gas to go through, which weakens the backflow. Varying the distance of the catalyst bed post-plasma can to some degree affect the strength of the backflow. However, based on the results, the combined effect of backflow and catalytic activity in the T-bed configuration is still negligible compared with the effect in the N-bed configuration with α-Al_2O_3. To exclude the effect of the presence of the N-bed itself from the packing and catalyst effect, it was added to the GAP DRM without any catalysts or filling materials inside (as shown in Fig. S5). Compared with the plasma alone (no catalyst or α-Al_2O_3 filling material), the conversions of both CO_2 and CH_4 remained almost the same. This proved that the N-bed itself did not cause any backflow of plasma gas without the addition of packing materials (either α-Al_2O_3 or catalysts).

In the presence of the Ni/MO catalyst, the CO_2 conversion further improved to 79% and that of CH_4 increased to 91%. As the 1 g α-Al_2O_3 was replaced by 1 g Ni/MO catalyst with the same particle size, the distance between the catalyst or the α-Al_2O_3 and post-plasma are the same, suggesting the same gas backflow behaviour. Therefore, this improvement can be attributed to the thermal catalytic performance of the catalyst. In contrast to the T-bed, the design of the N-bed clearly benefits from the catalyst, due to the direct connection of catalyst bed to the plasma device, helping the transfer of heat and mass from the plasma to the catalyst bed, which contributes to the heating of the catalyst. Furthermore, the metal connector helps the heat transfer from the electrode to the catalyst bed as well. Moreover, just like in the N-bed α-Al_2O_3 case, all the feed gas flows through the catalyst, while in the T-bed, some gas tends to go through the path of least resistance or pressure drop, which means part of the gas would pass directly from the side part of the T-bed rather than passing through the catalyst. This decreases the contact between feed gas and catalyst and finally leads to very limited, if any, catalytic activity. An additional positive effect might result from the double walled configuration formed by the N-bed and the post-plasma cylinder (Fig. 1B), in which the catalyst bed is embedded in a larger outer quartz reactor tube containing exhaust gas of the catalyst bed. This might insulate the heat of the N-bed part to some extent as also visible by the temperature differences at 4.9 cm for the T-bed and N-bed configuration in Fig. 4 (right y-axis, 233–284 °C vs. 462–524 °C). Although, without the catalyst or α-Al_2O_3 filling material, this insulation (formed by the double-wall of the N-bed and inside the quartz wall) seems insufficient, as deduced from the experiment with the empty N-bed. As the N-bed is placed at a close distance after the GAP plasma exhaust, the long-lived plasma-excited species may possibly contribute to the improved conversion. However, at the flow rates applied, at least around 0.2 s would be required for the species to reach the catalyst bed, which is longer than the lifetime of excited plasma species (millisecond range) [6, 55]. This means that all radicals have recombined before reaching the catalyst, and they do not directly interact with the catalyst surface. In addition, the heat released upon their recombination (change in enthalpy) is already included in the "hot gas" reaching the catalyst. In other words, the plasma acts as a heat source for post-plasma thermal

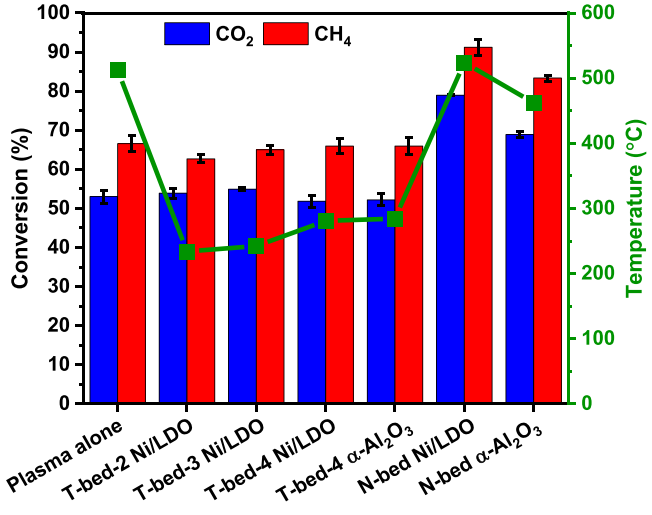

Fig. 4. Conversions (left y-axis) of CH_4 and CO_2 and the temperature (right y-axis, green line) at 4.9 cm after plasma 15 min at different GAP post-plasma catalyst configurations. Gas composition: N_2, CH_4, CO_2; GHSV: 480 $L \cdot g_{cat}^{-1} \cdot h^{-1}$.

catalysis. Moreover, the molecules reaching the catalyst are different from the classical thermal process as it consists of the composition formed in the plasma and plasma exhaust (recombination products). To reveal the role of reactive plasma species in our case in more detail, computer simulations could offer valuable insights, but developing such models is very challenging and outside the scope of this paper.

The temperature at 4.9 cm post-plasma was measured by a thermocouple (see Fig. 1B-C), which was placed after the catalyst bed once the catalyst was added. The temperature data shown in Fig. 4 (right y-axis) illustrates that a higher temperature was achieved in the N-bed configuration, i.e., around 462 °C during the reaction process for the Ni/MO catalyst, and even around 524 °C for the α-Al_2O_3. In the T-bed-3 Ni/MO catalyst case, the temperature was only around 233–284 °C. It indicates the temperature in the catalyst layer in the N-bed is higher than in the T-bed and this higher temperature promotes the catalyst, explaining its higher catalytic activity. Additionally, after reaction, a small amount of catalyst was found aggregated either together or with the filling material in the N-bed case, which can be due to the high temperature. However, this phenomenon did not appear in the T-bed. As shown in Fig. S3C, in the T-bed case with insulation, the temperature after the catalyst bed can reach about 450 °C, similar with that in the N-bed with Ni/MO, however, the latter had improved performance for GAP DRM. This illustrates that the design of the N-bed, which can cause better mass and heat transfer and might have a different impact on flow behaviour (feed gas pressure changed from 0.25 bar to 0.3 bar, meausred by the pressure gauge in Fig. S1), plays a crucial role for the enhancements. Moreover, the fact that for α-Al_2O_3 in the N-bed, the temperature was higher than for the Ni/MO catalyst proves the catalytic effect of the catalyst, as DRM is an endothermic reaction, which leads to a decrease in the temperature. This phenomenon also appeared in the configuration with a CH_4/CO_2 ratio of 0.6 (Fig. S5).

In contrast with the CH_4 and CO_2 conversion, which were little affected by the position of the catalyst in the T-bed, the selectivity of H_2 and by-products (C_2H_2 and C_2H_4) varied significantly, as shown in Fig. 5A-B. With the addition of the T-bed, at 2 cm, the selectivity of CO decreased from 69% to 66%, whereas that of H_2 increased from 79% to 89% at this position. By increasing the distance to 3 cm and 4 cm, the selectivity of CO kept almost unchanged, whereas the H_2 selectivity decreased a bit to around 80%, i.e., to almost the same value as without T-bed and catalyst. When using the N-bed without catalyst, the selectivity to H_2 was 78%, i.e., almost the same as with the plasma alone configuration. However, the selectivity to CO was clearly enhanced from 69% for plasma alone to 89% for the α-Al_2O_3 filled N-bed. A further increase of the CO and H_2 selectivity was obtained with the addition of Ni/MO catalyst, resulting in the highest selectivity value of 96% for CO and 92% for H_2, respectively. This can be due to the facilitating effect of the N-bed, which improves the mass and heat transfer to the catalyst and eventually promotes the catalyst, explaining its higher catalytic activity.

An increase in the selectivity to C_2H_2 from 18% to 20–22% was observed when the T-bed was added (cf. Fig. 5B). Changing the distance and filling material (catalyst or α-Al_2O_3) caused the C_2H_2 selectivity values to fluctuate around 21%, suggesting that the configurations like distance and catalyst had limited effect on the C_2H_2 selectivity in the T-bed cases. However, the selectivity to C_2H_2 dropped from around 20–22% for plasma alone and the T-bed configurations, to 4% for the N-bed with Ni/MO catalyst and to 12% for the N-bed with α-Al_2O_3. The same decreasing trend happened for the C_2H_4 selectivity which declined from around 1.6% (T-bed cases) to 0.4% (N-bed with Ni/MO) and 0.8% (N-bed with α-Al_2O_3). These changes are in accordance with the selectivity enhancing trend of CO and H_2. On the one hand, this can be

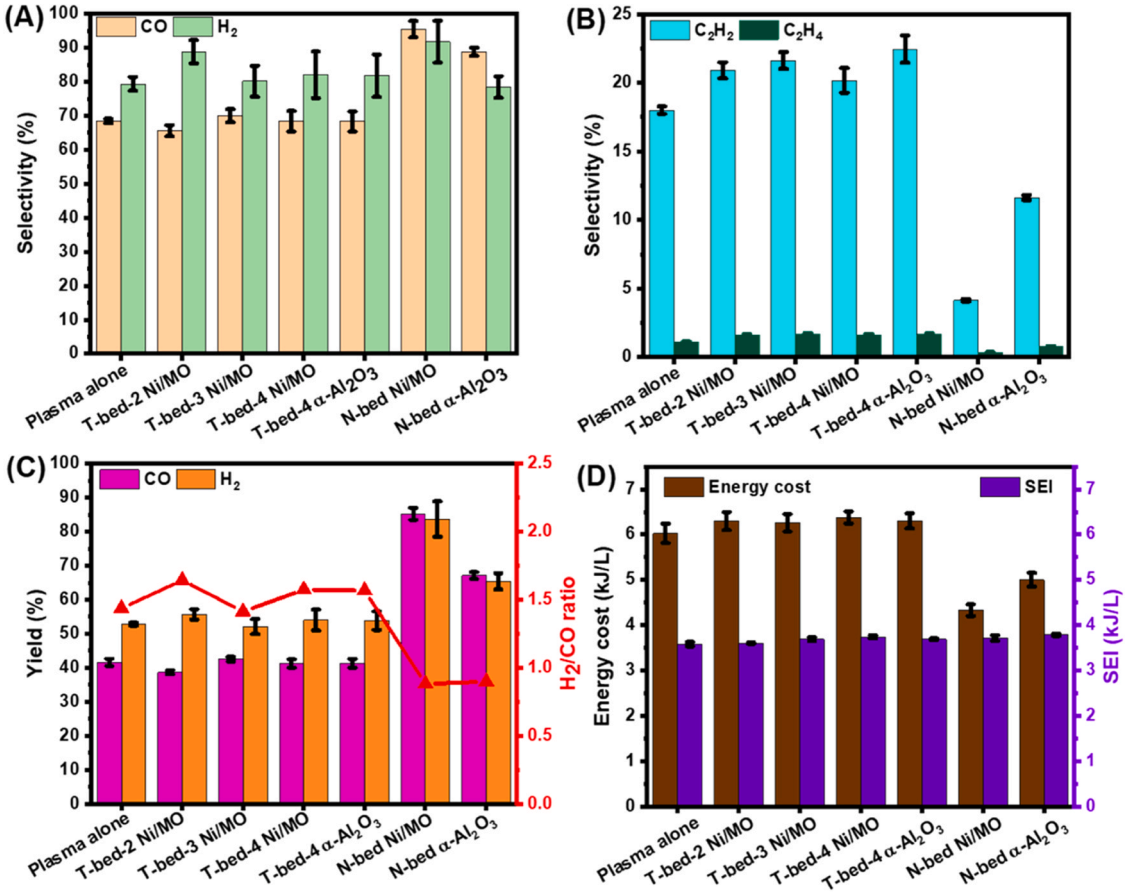

Fig. 5. (A) Selectivity of CO and H_2, (B) Selectivity of C_2H_2 and C_2H_4, (C) Yield of CO and H_2 and the H_2/CO ratio, and (D) Energy cost of the conversion (left y-axis) and specific energy input (SEI) into the system (right y-axis) in different cases. Gas composition: N_2:CH_4:CO_2 = 8:1:1, GHSV: 480 $L{\cdot}g_{cat}^{-1}h^{-1}$.

attributed to the catalytic effect performed by the catalyst. On the other hand, the efficient transfer of heat from the plasma to the inside region of the catalyst bed may cause a higher temperature environment which may be not beneficial for the production of relatively unstable products like C_2H_2 and C_2H_4. Moreover, also the backflow of gas into the plasma afterglow, containing reactive species, might provide a positive effect.

The yield of CO and H_2 (Fig. 5 C) shows that the highest yields were achieved in the N-bed case with catalyst, yielding 85% for CO and 84% for H_2, respectively, while in the T-bed, for all cases, the CO and H_2 yields were very similar as in the plasma alone case. However the H_2/CO ratio increased to 1.6 (for T-bed with catalyst at a distance of 2 cm), as compared to 1.4 in plasma alone configuration, due to the increase of selectivity towards H_2. However, with the N-bed, the H_2/CO ratio was lower than 1 (0.88 for N-bed with Ni/MO, and 0.89 for N-bed with α-Al_2O_3). This can be attributed to two reasons. Firstly, the catalytic effect of the catalyst promotes the CO_2 conversion and thus produces more CO (see the thermal DRM result in Fig. 3). In addition, some deposited carbon might be converted into CO as the carbon balance increased to around 100% in the N-bed configuration (Fig. S7A).

The specific energy input (SEI) for the various configurations was plotted in Fig. 5D (right y-axis), and illustrates that compared with plasma alone, upon addition of the catalyst bed, no matter T-bed or N-bed, the SEI is almost constant around the values of 3.6 – 3.8 kJ/L, as the plasma power and flow were constant. Therefore, since the conversions barely changed in the T-bed at different positions with Ni/MO catalyst or α-Al_2O_3, the energy cost was stable in the range of 6.3–6.4 kJ/L (see Fig. 5D: left y-axis). As the N-bed improves the plasma-catalytic conversions of CO_2 and CH_4, the energy cost values for the plasma catalytic process are lower, at 5.0 kJ/L in case of α-Al_2O_3 and 4.3 kJ/L for the Ni/MO catalyst. These results demonstrate that the N-bed can efficiently improve the GAP post-plasma catalytic DRM reaction.

Considering the catalyst can deactivate due to the carbon deposition, which may also happen in this plasma-catalytic DRM system, the hypothesis was verified whether the catalyst can already deactivate due to carbon deposition at the early plasma start up, before the temperature was reached at which the catalyst was active. For this reason, experiments with a lower CH_4/CO_2 ratio of 0.6 (gas composition: N_2:CH_4:CO_2 = 8:0.6:1) were done to compare the performance of the catalyst in the different catalyst beds (results see Figs. S5–6). The results indicate that this is probably not the reason why the T-bed is not working properly (see conversion, selectivity, yield, SEI and energy cost data in Figs. S5–6). The temperature after the T-bed and N-bed was collected as well (Fig. S5), showing that the gas temperature after the N-bed was also higher than that in T-bed (around 400 °C vs. 300 °C). Hence, the combined effects of the higher temperature, strong backflow or change in flow behaviour and double-walled insulation formed by the specially designed structure must be an important reason why the N-bed works well and the T-bed was inactive.

3.3.2. Carbon deposition and analysis

Nevertheless, carbon deposition is one of the main drawback for catalyst deactivation in DRM. Therefore, it is meaningful to study the carbon deposition in the plasma-catalytic DRM. The carbon balance of the plasma alone and coupled with catalysts for the different types of catalyst bed configurations for DRM are shown in Table S2. It can be noticed that reducing the CH_4/CO_2 ratio from 1 to 0.6 can decrease the loss of carbon, which, in the plasma alone case, increases from 93% to 99%. This difference became negligible in the N-bed cases as the carbon balance was 100% in both cases. Moreover, in the plasma alone or with T-bed configurations at CH_4/CO_2 ratio of 1, some carbon can be collected by paper on the inside wall of the post-plasma tube, which became negligible in the N-bed configurations.

TG in O_2 gas coupled with MS was used to analyze the amount of carbon deposition on the catalyst after about 35–45 min of DRM reaction in the different reactor configurations at a CH_4/CO_2 ratio of 1 (Fig. 6). Combined with the DTG result in Fig. S8A, it can be seen that

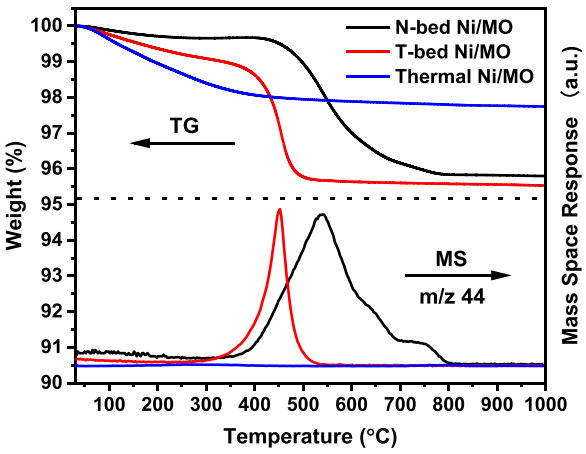

Fig. 6. TG, DTG and the MS results of Ni/MO catalyst obtained after DRM reaction in different reactor configurations (In T-bed plasma configuration, the reaction time is around 35 min, in N-bed configuration, the reaction time is around 45 min, and in the thermal catalytic reaction, the reaction time is the entire temperature range procedure). Gas composition: N_2:CH_4:CO_2 = 8:1:1, GHSV: 480 $L{\cdot}g_{cat}^{-1}h^{-1}$.

there was only about 2% total weight loss for thermal utilized Ni/MO catalyst at a temperature below about 400 °C. Enlarging the result of MS *m/z*=44 (Fig. S8B) indicates two peaks of CO_2 in the temperature of 100–500 °C and 700–850 °C. MS results of *m/z*=28 and 18 (Fig. S8C) suggest the presence of H_2O and absence of CO as part of the weight loss. Much more weight loss was observed in both T-bed and N-bed post-plasma configurations. In the T-bed configuration, carbon was lost in a temperature range of around 300 °C up to about 550 °C, coinciding with about 3.6% weight loss. MS data of *m/z* of 28 and 18 show that a small amount of CO was formed, visible from the sharp peak at around 400–500 °C, while no H_2O signal was observed in this temperature range. Similar phenomena were found in the N-bed case although with some difference. The weight loss occurred in a larger temperature range of around 350–800 °C with 3.8% weight loss and the CO peak was wider from about 420 °C to 650 °C. The TG results suggest that the carbon deposited on the catalyst mixture in the N-bed configuration had stronger interaction than those in the thermal catalytic or T-bed configurations or that the type of carbon formed was different. Furthermore, although in the thermal catalytic DRM, the least carbon deposition was found, the carbon balance was only 89%, which is lower than the 96% in the T-bed and 100% in the N-bed configurations. Several reasons may lead to this. A possible reason is that for the TG process, around 100 mg mixture of Ni/MO catalyst and α-Al_2O_3 sample was utilized, while this implies only 1/11 wt of catalyst in the thermal catalytic case (as 10 mg catalyst was mixed with 100 mg α-Al_2O_3) and in T-bed and N-bed configurations this value is 1/5 (as 1 g catalyst mixed with 4 g α-Al_2O_3). Assuming all the carbon would be deposited on the catalyst, after correction, the carbon deposition should be around 4.4%, a bit higher than those in the T-bed and N-bed configurations. Besides this, considering the carbon balance in N-bed configuration was 100%, this conflicted with the carbon loss in TG-MS. This could be caused by the carbon deposition before the plasma reaches its maximum conversion and thus temperature. Furthermore, as the internal standard gas N_2 was present in the feed gas, it may lead to some larger error on the results. Hence, the underlying reasons are not yet fully clear and require more research, which is outside of the scope of this paper, focusing on the benefits of the N-bed versus the T-bed.

The carbon collected in the plasma cases was further studied via Raman spectra (Fig. 7). The spectra of the samples all exhibited typical carbon signals at around 1346 cm^{-1} (D band) and 1574 cm^{-1} (G band), whereas the G band peak shifted to a higher wavenumber (1586 cm^{-1}) for the N-bed and an even higher wavenumber (1601 cm^{-1}) for T-bed.

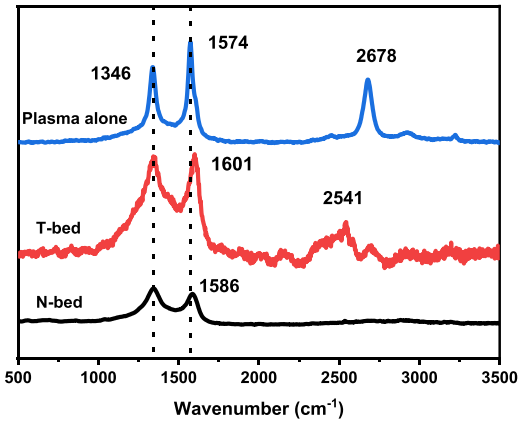

Fig. 7. Raman spectra of carbon produced under plasma or plasma-catalytic conditions.

Furthermore, the spectrum for plasma alone showed a 2D band (2678 cm^{-1}), attributed to the overtone of the D band.

The ratio of relative intensity of the D band to the G band (I_D/I_G) in the Raman spectrum (Fig. 7) is commonly used to quantify the defects and crystallinity of graphene samples. The low value of I_D/I_G indicates a high degree of graphitization of the samples [40,63,64]. For the three cases, the I_D/I_G values were approximately 0.79 for plasma alone case, 0.97 for T-bed case, and 1.12 the for N-bed case, showing a decreasing trend of graphitization of the carbon formed.

3.4. Comparison of DRM results with various plasma configurations

The reactant conversion, product selectivity, and energy cost are important parameters to evaluate the performance of plasma-catalytic DRM. Therefore, we list these performance data in Table 1, along with the experimental conditions (catalyst (if used), CH_4/CO_2 ratio, gas flow rate, and plasma power), for various plasma reactors reported in literature. It is clear that our obtained conversion of CH_4 and CO_2 are higher than most of the reported values for GA, RGA, DBD, sparking plasma and MW plasma, while at a significantly lower energy cost and using a higher gas flow rate. Although in the GA plasma with extra external heating to 850 °C, the conversion of CH_4 and CO_2 and the selectivity to CO and H_2 were higher [50], the energy cost was about 6 times higher. Considering the catalytic performance, our GAP post-plasma-catalytic DRM reaction with N-bed and Ni/MO catalyst is competitive to the current state of the art.

4. Conclusion

We present a GAP plasma reactor in combination with a newly designed catalyst bed, containing a Ni/MO catalyst derived from LDH, for post-plasma-catalytic dry reforming of methane. The catalytic activity of the catalyst was evaluated and compared with a traditional fixed bed for thermal catalytic DRM and a maximum 96% CH_4 and 86% CO_2 conversion was achieved at 800 °C. For the post-plasma-catalytic DRM reaction, two types of catalyst bed configurations (tray-type T-bed and newly designed N-bed) were applied to study how the catalyst bed design affects the results. We found that using a traditional catalyst bed (T-bed) had little effect on the conversion of CO_2 and CH_4, while the use of the newly designed catalyst bed (N-bed) can efficiently enhance both CO_2 and CH_4 conversion, and CO and H_2 selectivity, and decrease the energy cost at the same time, without external insulation or heating, providing a true, fully electrically driven process, transferring the heat produced in the plasma to the post-plasma catalysis. When using a CH_4/CO_2 ratio of 1, the highest conversions of CO_2 of 79% and CH_4 of 91%, in combination with a vast increase in selectivity to CO (96%) and H_2 (91%), were obtained in the N-bed with Ni/MO catalyst present, which are comparable to those achieved in the thermal catalytic DRM at 800 °C. This improvement was proven to be caused by the catalytic activity of the catalyst, which was facilitated by the direct connection of the N-bed to the GAP plasma device, transferring more heat from the GAP device, activating the catalyst, while also providing beneficial mass transfer and flow behaviour. The latter was deduced from the improved performance in the presence of α-Al_2O_3 filling in the absence of catalytic material, in combination with the lack of enhanced performance in case of an empty N-bed connected to the plasma.

To our knowledge, this is the first time that excellent catalytic activity in a PPC system was observed without requiring extra external heating or insulation, which indeed illustrates the high potential of PPC systems towards process electrification and plasma energy, *i.e.* heat, recovery.

Author contributions

Wencong Xu performed the materials synthesis and characterization, thermal and plasma DRM reactions, data analysis, the paper writing-original draft and conceptualization. Lukas C. Buelens performed thermal DRM, data analysis, review, and editing. Vladimir V. Galvita performed writing, review, editing, supervision and funding. Annemie

Table 1
Operating conditions, CH_4/CO_2 conversion, CO/H_2 selectivity and energy cost in various plasma reactors for DRM.

Plasma	Catalyst	CH_4/CO_2	Power (W)	Total flow rate (L/min)	Conversion		Selectivity		Energy cost[a] (kJ/L)	Ref.
					CH_4	CO_2	CO	H_2		
GA	-	3:7	165	7.5	13.1	8.4	31.4	69.5	14.4	[40]
RGA	Ni/γ-Al_2O_3[b]	3:7	490	6	58.5	39.5	56	35.3	13	[34]
GA (heating 850 °C)	Ni-based catalyst[b]	1:1	494	2.67	94	91	95	97	26.7[d]	[50]
RGA	15 wt% NiO-Al_2O_3[b]	2:3	136	3.7	11.8	11.2	88.1	75.3	40.2	[42]
RGA	-	1:1	1800	24	50.5	40.3	81.2	83.5	18.5	[43]
Glow discharge	-	1:3	n/a	1	94	64	n/a	n/a	17	[13]
DBD	Ni-based metal oxide[c]	1:1	33–38	0.03	69	54	74.5	62.5	n/a	[65]
Sparking plasma	Ferroelectric ($BaZr_{0.05}Ti_{0.95}O_3$)[c]	1:1	39	0.2	86	82.4	67.4	88.7	9.8	[66]
MW	-	1:2	700	2.1	79.4	44.8	58.4	50.1	n/a	[24]
GAP	Ni-based metal oxide[b]	1:1	508	8	91	79	95	92	4.3	This work

GA: gliding arc plasma; RGA: rotating gliding arc plasma; DBD: dielectric barrier discharge plasma; MW: microwave plasma; GAP: gliding arc plasmatron.
n/a: Data not reported or could not be determined from the data mentioned in the paper.
[a] Some energy cost data were reported in different units, therefore, they were calculated into the same unit, except Ref. [14,44] which were the data as reported.
[b] Post-plasma catalysis (PPC) model;
[c] In-plasma catalysis (IPC) model;
[d] The energy cost calculated based on CO_2 and including both plasma energy cost and additional heating energy cost.

Bogaerts performed writing, review, editing, conceptualization, supervision and funding. Vera Meynen performed writing, review, editing, conceptualization, supervision and funding.

CRediT authorship contribution statement

Vera Meynen: Writing – review & editing, Supervision, Project administration. **Annemie Bogaerts:** Writing – review & editing, Supervision. **Vladimir V. Galvita:** Writing – review & editing, Supervision. **Lukas C. Buelens:** Writing – review & editing, Formal analysis, Data curation. **Wencong Xu:** Writing – original draft, Methodology, Investigation, Funding acquisition, Formal analysis, Data curation, Conceptualization.

Declaration of Competing Interest

The authors declare that they have no known competing financial interests or personal relationships that could have appeared to influence the work reported in this paper.

Data availability

Data will be made available on request.

Acknowledgments

Wencong Xu, Vladimir V. Galvita, Annemie Bogaerts, and Vera Meynen would like to acknowledge the VLAIO Catalisti Moonshot project D2M and the VLAIO Catalisti transition project CO2PERATE (HBC.2017.0692). Lukas C. Buelens acknowledges financial support from the Fund for Scientific Research Flanders (FWO Flanders) through a postdoctoral fellowship grant 12E5623N. Vladimir V. Galvita also acknowledges a personal grant from the Research Fund of Ghent University (BOF; 01N16319).

Appendix A. Supporting information

Supplementary data associated with this article can be found in the online version at doi:10.1016/j.jcou.2024.102820.

References

[1] E. le Saché, T.R. Reina, Analysis of dry reforming as direct route for gas phase CO2 conversion. The past, the present and future of catalytic DRM technologies, Prog. Energy Combust. Sci. 89 (2022) 100970, https://doi.org/10.1016/j.pecs.2021.100970.

[2] A. Mustafa, B.G. Lougou, Y. Shuai, Z. Wang, H. Tan, Current technology development for CO2 utilization into solar fuels and chemicals: a review, J. Energy Chem. 49 (2020) 96–123, https://doi.org/10.1016/j.jechem.2020.01.023.

[3] I.V. Yentekakis, P. Panagiotopoulou, G. Artemakis, A review of recent efforts to promote dry reforming of methane (DRM) to syngas production via bimetallic catalyst formulations, Appl. Catal. B Environ. 296 (2021) 120210, https://doi.org/10.1016/j.apcatb.2021.120210.

[4] N. Anoop, S. Sundaramurthy, J.M. Jha, S. Chandrabalan, N. Singh, J. Verma, D. Parvatalu, S. Katti, Plasma catalysis: a feasible solution for carbon dioxide valorization, Clean. Technol. Environ. Policy 23 (2021) 2789–2811, https://doi.org/10.1007/s10098-021-02203-y.

[5] G. Chen, R. Snyders, N. Britun, CO2 conversion using catalyst-free and catalyst-assisted plasma-processes: recent progress and understanding, J. CO2 Util. 49 (2021) 101557, https://doi.org/10.1016/j.jcou.2021.101557.

[6] V. Vermeiren, A. Bogaerts, Plasma-based CO2 conversion: to quench or not to quench, J. Phys. Chem. C. 124 (2020) 18401–18415.

[7] A. George, B. Shen, M. Craven, Y. Wang, D. Kang, C. Wu, X. Tu, A review of non-thermal plasma technology: a novel solution for CO2 conversion and utilization, Renew. Sustain. Energy Rev. 135 (2021) 109702, https://doi.org/10.1016/j.rser.2020.109702.

[8] S. Van Alphen, J. Slaets, S. Ceulemans, M. Aghaei, R. Snyders, A. Bogaerts, Effect of N2 on CO2-CH4 conversion in a gliding arc plasmatron: can this major component in industrial emissions improve the energy efficiency, J. CO2 Util. 54 (2021) 101767, https://doi.org/10.1016/j.jcou.2021.101767.

[9] D. Mei, G. Duan, J. Fu, S. Liu, R. Zhou, R. Zhou, Z. Fang, P.J. Cullen, K. (Ken Ostrikov, CO2 reforming of CH4 in single and double dielectric barrier discharge reactors: comparison of discharge characteristics and product distribution, J. CO2 Util. 53 (2021) 101703, https://doi.org/10.1016/j.jcou.2021.101703.

[10] Y. Wang, Y. Chen, J. Harding, H. He, A. Bogaerts, X. Tu, Catalyst-free single-step plasma reforming of CH4 and CO2 to higher value oxygenates under ambient conditions, Chem. Eng. J. 450 (2022) 137860, https://doi.org/10.1016/j.cej.2022.137860.

[11] J. Pan, T. Chen, Y. Gao, Y. Liu, S. Zhang, Y. Liu, T. Shao, Numerical modeling and mechanism investigation of nanosecond-pulsed DBD plasma-catalytic CH4 dry reforming, J. Phys. D. Appl. Phys. 55 (2022) 035202, https://doi.org/10.1088/1361-6463/ac2ad8.

[12] K. Pornmai, S. Suvachitanont, S. Chavadej, Reforming of CO2-containing natural gas with steam in AC gliding arc discharge for hydrogen production, Int. J. Green. Energy 15 (2018) 441–453, https://doi.org/10.1080/15435075.2018.1475285.

[13] B. Wanten, S. Maerivoet, C. Vantomme, J. Slaets, G. Trenchev, A. Bogaerts, Dry reforming of methane in an atmospheric pressure glow discharge: confining the plasma to expand the performance, J. CO2 Util. 56 (2022) 101869, https://doi.org/10.1016/j.jcou.2021.101869.

[14] Z. Sheng, Y. Watanabe, H.H. Kim, S. Yao, T. Nozaki, Plasma-enabled mode-selective activation of CH4 for dry reforming: first touch on the kinetic analysis, Chem. Eng. J. 399 (2020) 125751, https://doi.org/10.1016/j.cej.2020.125751.

[15] D. Mei, P. Zhang, G. Duan, S. Liu, Y. Zhou, Z. Fang, X. Tu, CH4 reforming with CO2 using a nanosecond pulsed dielectric barrier discharge plasma, J. CO2 Util. 62 (2022) 102073, https://doi.org/10.1016/j.jcou.2022.102073.

[16] J. Wang, K. Zhang, A. Bogaerts, V. Meynen, 3D porous catalysts for plasma-catalytic dry reforming of methane: how does the pore size affect the plasma-catalytic performance, Chem. Eng. J. 464 (2023) 142574, https://doi.org/10.1016/j.cej.2023.142574.

[17] X. Chen, H.H. Kim, T. Nozaki, Plasma catalytic technology for CH4 and CO2 conversion: a review highlighting fluidized-bed plasma reactor, Plasma Process. Polym. (2023) e2200207, https://doi.org/10.1002/ppap.202200207.

[18] N. Bouchoul, E. Fourré, A. Duarte, N. Tanchoux, C. Louste, C. Batiot-Dupeyrat, Plasma-metal oxides coupling for CH4-CO2 transformation into syngas and/or hydrocarbons, oxygenates, Catal. Today 369 (2021) 62–68, https://doi.org/10.1016/j.cattod.2020.06.058.

[19] J. Wang, K. Zhang, V. Meynen, A. Bogaerts, Dry reforming in a dielectric barrier discharge reactor with non-uniform discharge gap: effects of metal rings on the discharge behavior and performance, Chem. Eng. J. 465 (2023) 142953, https://doi.org/10.1016/j.cej.2023.142953.

[20] E. Devid, D. Zhang, D. Wang, M. Ronda-Lloret, Q. Huang, G. Rothenberg, N. R. Shiju, A.W. Kleyn, Dry reforming of methane under mild conditions using radio frequency plasma, Energy Technol. 8 (2020) 1–10, https://doi.org/10.1002/ente.201900886.

[21] Z. Liu, B. Huang, W. Zhu, C. Zhang, X. Tu, T. Shao, Phase-resolved measurement of atmospheric-pressure radio-frequency pulsed discharges in Ar/CH4/CO2 mixture, Plasma Chem. Plasma Process. 40 (2020) 937–953, https://doi.org/10.1007/s11090-020-10071-5.

[22] J. Xu, Y. Liu, H. Tian, Q. Zhang, W. Cao, K. Chen, F. Guo, Ni-based catalysts with coke resistance enhance by radio frequency discharge plasma for CH4/CO2 reforming, Int. J. Hydrog. Energy 47 (2022) 5240–5249, https://doi.org/10.1016/j.ijhydene.2021.11.131.

[23] D. Li, X. Li, M. Bai, X. Tao, S. Shang, X. Dai, Y. Yin, CO2 reforming of CH4 by atmospheric pressure glow discharge plasma: a high conversion ability, Int. J. Hydrog. Energy 34 (2009) 308–313, https://doi.org/10.1016/j.ijhydene.2008.10.053.

[24] N.M. Alawi, J. Sunarso, G.H. Pham, A. Barifcani, M.H. Nguyen, S. Liu, Comparative study on the performance of microwave-assisted plasma DRM in nitrogen and argon atmospheres at a low microwave power, J. Ind. Eng. Chem. 85 (2020) 118–129, https://doi.org/10.1016/j.jiec.2020.01.032.

[25] H. Sun, J. Lee, M.S. Bak, Experiments and modeling of atmospheric pressure microwave plasma reforming of a methane-carbon dioxide mixture, J. CO2 Util. 46 (2021) 101464, https://doi.org/10.1016/j.jcou.2021.101464.

[26] F. Zhang, X. Zhang, Z. Song, X. Li, X. Zhao, J. Sun, Y. Mao, X. Wang, W. Wang, Promotion of microwave discharge over carbon catalysts for CO2 reforming of CH4 to syngas, Fuel 331 (2023) 125914, https://doi.org/10.1016/j.fuel.2022.125914.

[27] A. Bogaerts, C. De Bie, R. Snoeckx, T. Kozák, Plasma based CO2 and CH4 conversion: a modeling perspective, Plasma Process. Polym. 14 (2017) e1600070, https://doi.org/10.1002/ppap.201600070.

[28] A. Aziznia, H.R. Bozorgzadeh, N. Seyed-Matin, M. Baghalha, A. Mohamadalizadeh, Comparison of dry reforming of methane in low temperature hybrid plasma-catalytic corona with thermal catalytic reactor over Ni/γ-Al2O3, J. Nat. Gas. Chem. 21 (2012) 466–475, https://doi.org/10.1016/S1003-9953(11)60392-7.

[29] H.H. Nguyen, A. Nasonova, I.W. Nah, K.S. Kim, Analysis on CO2 reforming of CH4 by corona discharge process for various process variables, J. Ind. Eng. Chem. 32 (2015) 58–62, https://doi.org/10.1016/j.jiec.2015.07.018.

[30] J. Slaets, M. Aghaei, S. Ceulemans, S. Van Alphen, A. Bogaerts, CO2 and CH4 conversion in "real" gas mixtures in a gliding arc plasmatron: how do N2 and O2 affect the performance, Green. Chem. 22 (2020) 1366–1377, https://doi.org/10.1039/c9gc03743h.

[31] E. Cleiren, S. Heijkers, M. Ramakers, A. Bogaerts, Dry reforming of methane in a gliding arc plasmatron: towards a better understanding of the plasma chemistry, ChemSusChem 10 (2017) 4025–4036, https://doi.org/10.1002/cssc.201701274.

[32] N. Lu, D. Sun, Y. Xia, K. Shang, B. Wang, N. Jiang, J. Li, Y. Wu, Dry reforming of CH4–CO2 in AC rotating gliding arc discharge: effect of electrode structure and gas parameters, Int. J. Hydrog. Energy 43 (2018) 13098–13109, https://doi.org/10.1016/j.ijhydene.2018.05.053.

[33] R. Xu, X. Kong, H. Zhang, P.M. Ruya, X. Li, Destruction of gasification tar over Ni catalysts in a modified rotating gliding arc plasma reactor: effect of catalyst position and nickel loading, Fuel 289 (2021) 119742, https://doi.org/10.1016/j.fuel.2020.119742.
[34] F. Zhu, H. Zhang, X. Yan, J. Yan, M. Ni, X. Li, X. Tu, Plasma-catalytic reforming of CO2-rich biogas over Ni/γ-Al2O3 catalysts in a rotating gliding arc reactor, Fuel 199 (2017) 430–437, https://doi.org/10.1016/j.fuel.2017.02.082.
[35] J.L. Liu, Z.W. Xue, Z.Y. Zhang, B. Sun, A.M. Zhu, Mechanism study on gliding arc (GA) plasma reforming: unraveling the decisive role of CH4/CO2 ratio in the dry reforming reaction, Plasma Process. Polym. (2022) e2200175, https://doi.org/10.1002/ppap.202200175.
[36] M. Ramakers, G. Trenchev, S. Heijkers, W. Wang, A. Bogaerts, Gliding arc plasmatron: providing an alternative method for carbon dioxide conversion, ChemSusChem 10 (2017) 2642–2652, https://doi.org/10.1002/cssc.201700589.
[37] R. Snoeckx, A. Bogaerts, Plasma technology-a novel solution for CO2 conversion, Chem. Soc. Rev. 46 (2017) 5805–5863, https://doi.org/10.1039/c6cs00066e.
[38] J. Feng, X. Sun, Z. Li, X. Hao, M. Fan, P. Ning, K. Li, Plasma-assisted reforming of methane, Adv. Sci. 9 (2022) 1–36, https://doi.org/10.1002/advs.202203221.
[39] Z.A. Allah, J.C. Whitehead, Plasma-catalytic dry reforming of methane in an atmospheric pressure AC gliding arc discharge, Catal. Today 256 (2015) 76–79, https://doi.org/10.1016/j.cattod.2015.03.040.
[40] X. Tu, J.C. Whitehead, Plasma dry reforming of methane in an atmospheric pressure AC gliding arc discharge: Co-generation of syngas and carbon nanomaterials, Int. J. Hydrog. Energy 39 (2014) 9658–9669, https://doi.org/10.1016/j.ijhydene.2014.04.073.
[41] Z. Bo, J. Yan, X. Li, Y. Chi, K. Cen, Plasma assisted dry methane reforming using gliding arc gas discharge: effect of feed gases proportion, Int. J. Hydrog. Energy 33 (2008) 5545–5553, https://doi.org/10.1016/j.ijhydene.2008.05.101.
[42] J. Martin-Del-Campo, M. Uceda, S. Coulombe, J. Kopyscinski, Plasma-catalytic dry reforming of methane over Ni-supported catalysts in a rotating gliding arc - Spouted bed reactor, J. CO2 Util. 46 (2021) 101474, https://doi.org/10.1016/j.jcou.2021.101474.
[43] H. Kwon, T. Kim, S. Song, Dry reforming of methane in a rotating gliding arc plasma: improving efficiency and syngas cost by quenching product gas, SSRN Electron. J. 70 (2022) 102448, https://doi.org/10.2139/ssrn.4302968.
[44] T. Nunnally, K. Gutsol, A. Rabinovich, A. Fridman, A. Kemoun, Dissociation of CO2 in a low current gliding arc plasmatron, J. Phys. D. Appl. Phys. 44 (2011) 274009, https://doi.org/10.1088/0022-3727/44/27/274009.
[45] X. Lin, R. Li, M. Lu, C. Chen, D. Li, Y. Zhan, L. Jiang, Carbon dioxide reforming of methane over Ni catalysts prepared from Ni-Mg-Al layered double hydroxides: Influence of Ni loadings, Fuel 162 (2015) 271–280, https://doi.org/10.1016/j.fuel.2015.09.021.
[46] L. Jin, B. Ma, S. Zhao, X. He, Y. Li, H. Hu, Z. Lei, Ni/MgO–Al2O3 catalyst derived from modified [Ni,Mg,Al]-LDH with NaOH for CO2 reforming of methane, Int. J. Hydrog. Energy 43 (2018) 2689–2698, https://doi.org/10.1016/j.ijhydene.2017.12.087.
[47] M. Abbas, U. Sikander, M.T. Mehran, S.H. Kim, Exceptional stability of hydrotalcite derived spinel Mg(Ni)Al2O4 catalyst for dry reforming of methane, Catal. Today 403 (2022) 74–85, https://doi.org/10.1016/j.cattod.2021.08.029.
[48] H. Zhang, L. Li, R. Xu, J. Huang, N. Wang, X. Li, X. Tu, Plasma-enhanced catalytic activation of CO2 in a modified gliding arc reactor, Waste Dispos. Sustain. Energy 2 (2020) 139–150, https://doi.org/10.1007/s42768-020-00034-z.
[49] K. Li, J.L. Liu, X.S. Li, X. Zhu, A.M. Zhu, Warm plasma catalytic reforming of biogas in a heat-insulated reactor: dramatic energy efficiency and catalyst auto-reduction, Chem. Eng. J. 288 (2016) 671–679, https://doi.org/10.1016/j.cej.2015.12.036.
[50] J.L. Liu, Z. Li, J.H. Liu, K. Li, H.Y. Lian, X.S. Li, X. Zhu, A.M. Zhu, Warm-plasma catalytic reduction of CO2 with CH4, Catal. Today 330 (2019) 54–60, https://doi.org/10.1016/j.cattod.2018.05.046.
[51] H.Y. Lian, Z. Wei, S. Yun, R. Jing, L. Liu, Warm plasma catalytic coreforming of dilute bioethanol and methane for hydrogen production, Plasma Process. Polym. (2023) 1–9, https://doi.org/10.1002/ppap.202300062.
[52] E. Klemm, C.M.S. Lobo, A. Löwe, V. Schallhart, S. Renninger, L. Waltersmann, A.S. R. Dietrich, R. Costa, L. Möltner, V. Meynen, A. Sauer, K.A. Friedrich, CHEMampere: Technologies for sustainable chemical production with renewable electricity and CO2,N2,O2,and H2O, Can. J. Chem. Eng. 100 (2022) 2736–2761, https://doi.org/10.1002/cjce.24397.
[53] X. Lin, R. Li, M. Lu, C. Chen, D. Li, Y. Zhan, L. Jiang, Carbon dioxide reforming of methane over Ni catalysts prepared from Ni-Mg-Al layered double hydroxides: influence of Ni loadings, Fuel 162 (2015) 271–280, https://doi.org/10.1016/j.fuel.2015.09.021.
[54] W. Xu, M. Mertens, T. Kenis, E. Derveaux, P. Adriaensens, V. Meynen, Can high temperature calcined Mg–Al layered double hydroxides (LDHs) fully rehydrate at room temperature in vapor or liquid condition, Mater. Chem. Phys. 295 (2023) 127113, https://doi.org/10.1016/j.matchemphys.2022.127113.
[55] G. Trenchev, S. Kolev, W. Wang, M. Ramakers, A. Bogaerts, CO2 conversion in a gliding arc plasmatron: multidimensional modeling for improved efficiency, J. Phys. Chem. C. 121 (2017) 24470–24479, https://doi.org/10.1021/acs.jpcc.7b08511.
[56] M. Ramakers, S. Heijkers, T. Tytgat, S. Lenaerts, A. Bogaerts, Combining CO2 conversion and N2 fixation in a gliding arc plasmatron, J. CO2 Util. 33 (2019) 121–130, https://doi.org/10.1016/j.jcou.2019.05.015.
[57] Y. Zhan, K. Song, Z. Shi, C. Wan, J. Pan, D. Li, C. Au, L. Jiang, Influence of reduction temperature on Ni particle size and catalytic performance of Ni/Mg(Al)O catalyst for CO2 reforming of CH4, Int. J. Hydrog. Energy 45 (2020) 2794–2807.
[58] Y. Ren, Y.Y. Ma, W.L. Mo, J. Guo, Q. Liu, X. Fan, S.P. Zhang, Research progress of carbon deposition on Ni-based catalyst for CO2-CH4 reforming, Catalysts 13 (2023) 647, https://doi.org/10.3390/catal13040647.
[59] S.A. Theofanidis, V.V. Galvita, H. Poelman, G.B. Marin, Enhanced carbon-resistant dry reforming Fe-Ni catalyst: role of Fe, ACS Catal. 5 (2015) 3028–3039, https://doi.org/10.1021/acscatal.5b00357.
[60] N. Shah, P. Devadas, G.P. Huffman, Hydrogen production by catalytic decomposition of methane, Energy Fuels 15 (2001) 1528–1534, https://doi.org/10.1021/ef0101964.
[61] A.A. Abdulrasheed, A.A. Jalil, T.J. Siang, H.U. Hambali, Thermodynamic sensitivity analysis of CO2 reforming of methane based on equilibrium predictions, IOP Conf. Ser. Mater. Sci. Eng. 808 (2020), https://doi.org/10.1088/1757-899X/808/1/012001.
[62] J.L. Liu, Z. Li, J.H. Liu, K. Li, H.Y. Lian, X.S. Li, X. Zhu, A.M. Zhu, Warm-plasma catalytic reduction of CO2 with CH4, Catal. Today 330 (2019) 54–60, https://doi.org/10.1016/j.cattod.2018.05.046.
[63] D.L. Sun, R.Y. Hong, J.Y. Liu, F. Wang, Y.F. Wang, Preparation of carbon nanomaterials using two-group arc discharge plasma, Chem. Eng. J. 303 (2016) 217–230, https://doi.org/10.1016/j.cej.2016.05.098.
[64] H.M. Heise, R. Kuckuk, A. Srivastava, B.P. Asthana, Characterization of carbon nanotube filters and other carbonaceous materials by Raman spectroscopy-II: Study on dispersion and disorder parameters, J. Raman Spectrosc. 42 (2011) 294–302, https://doi.org/10.1002/jrs.2723.
[65] H. Wang, Y. Yang, Z. Li, X. Kong, P. Martin, G. Cui, R. Wang, Plasma-assisted Ni catalysts: toward highly-efficient dry reforming of methane at low temperature, Int. J. Hydrog. Energy 48 (2023) 8921–8931, https://doi.org/10.1016/j.ijhydene.2022.11.287.
[66] W.C. Chung, M.B. Chang, Dry reforming of methane by combined spark discharge with a ferroelectric, Energy Convers. Manag. 124 (2016) 305–314, https://doi.org/10.1016/j.enconman.2016.07.023.